Osteosarcoma : searching for new treatment options

Baranski Madrigal, Z.

2

Aven-mediated checkpoint kinase control regulates proliferation and resistance to chemotherapy in conventional osteosarcoma

Zuzanna Baranski, Tijmen H. Booij, Anne-Marie Cleton-Jansen, Leo Price, Bob van de Water, Judith V. M. G. Bovée, Pancras C.W. Hogendoorn, Erik H.J. Danen

Published in *J Pathol* **236**:348-359, 2015

ABSTRACT

Conventional high-grade osteosarcoma is the most common primary bone sarcoma with relatively high incidence in young people. Here, we found that expression of Aven is inversely correlated with metastasis-free survival in osteosarcoma patients and is increased in metastases compared to primary tumours. Aven is an adaptor protein that has been implicated in anti-apoptotic signaling and serves as an oncoprotein in acute lymphoblastic leukemia. In tumour cells, silencing Aven triggered a G2 cell cycle arrest. Chk1 protein levels were attenuated and ATR-Chk1 DNA damage response signaling in response to chemotherapy was abolished in Aven-depleted osteosarcoma cells while ATM, Chk2, and p53 activation remained intact. Osteosarcoma is notoriously difficult to treat with standard chemotherapy, and we examined whether pharmacological inhibition of the Aven-controlled ATR-Chk1 response could sensitize osteosarcoma cells to genotoxic compounds. Indeed, pharmacological inhibitors targeting Chk1/Chk2 or those selective for Chk1 synergized with standard chemotherapy in 2D cultures. Likewise, in 3D extracellular matrix-embedded cultures Chk1 inhibition led to effective sensitization to chemotherapy. Together, these findings implicate Aven in ATR-Chk1 signaling and point towards Chk1 inhibition as a strategy to sensitize human osteosarcomas to chemotherapy.

INTRODUCTION

Osteosarcoma is the most common primary malignant bone tumor occurring predominantly in children and adolescents, and a second peak at middle age. It is thought to arise from mesenchymal stem cells that are capable of producing osteoid [1,2]. At the moment of diagnosis, 10-20% of the patients present with metastasis. About 30-40% of the patients with localized osteosarcoma will relapse mainly by presenting lung metastasis. Patients with recurrence have very poor prognosis with 23-33% 5-year overall survival [3].

Aven is an adaptor protein that exerts anti-apoptotic activity by potentiating Bcl-xL and by interfering with the self-association of Apaf-1, thereby preventing the activation of caspase 9[4,5]. Aven has also been identified through bioinformatics analysis as a novel potential BH3-domain containing protein[6]. Besides being involved in apoptosis, Aven was reported to control the DNA damage response (DDR) by physically interacting with- and supporting the activity of “ataxia-telangiectasia mutated” (ATM)[7].

The DDR is evolutionary conserved and essential to ensure the faithful maintenance and replication of the genome. This elaborate integrated signaling cascade senses DNA damage and triggers repair, cell cycle arrest and, in case of severe damage, cell death. The serine/threonine protein kinases of the phosphatidylinositol 3-kinase-like family, ATM and “ATM and Rad3-related” (ATR) are crucial players in the DDR [8,9]. After DNA damage, ATM and ATR are activated and, in turn, they activate critical effectors, including components of the DNA damage repair machinery and the checkpoint kinases, Chk1 and Chk2 to arrest the cell cycle[10]. Combining cytotoxic chemotherapeutics with pharmacological Chk1/Chk2 inhibitors can prevent damaged cancer cells from arresting, causing increased tumor cell killing and thus, improved therapeutic efficacy [11].

In the context of cancer, Aven has thus far been exclusively implicated in hematopoietic malignancies. Aven mRNA levels have been associated with disease relapse and poor prognosis of acute lymphoblastic leukemia and Aven has been shown to act as an oncoprotein that drives proliferation and survival of leukemic cells [12-14]. Here, we analyze Aven mRNA, protein expression, and function in osteosarcoma, the most common primary bone malignancy that is very difficult to treat. We show that Aven expression is increased in metastatic lesions and inversely correlated with metastasis-free survival in osteosarcoma patients. We show that Aven is in fact dispensable for ATM-Chk2 (and p53) activation. Instead, Aven is required for ATR-Chk1 signaling and Aven silencing leads to G2 cell cycle

arrest. Moreover, in the absence of Aven osteosarcoma cells fail to activate Chk1 (but not Chk2) in response to DNA damaging chemotherapeutics. Finally, we show that targeting the Aven-controlled ATR-Chk1 activity using clinically relevant pharmacological inhibitors sensitizes osteosarcoma to chemotherapy.

MATERIALS AND METHODS

Reagents and antibodies. Doxorubicin was obtained from the Department of Clinical Pharmacology at LUMC, AZD7762 Chk1/Chk2 inhibitor. Ly2603618 and CHIR-124 selective Chk1 inhibitors were from SelleckChem (Huissen, Netherlands). Cisplatin and etoposide were from Sigma-Aldrich (Zwijndrecht, The Netherlands). Hoechst 33342 was purchased from Fischer Scientific (Bleiswijk, The Netherlands) and the pan-caspase inhibitor z-VAD-fmk was obtained from Bachem (Weil am Rhein, Germany). The Aven antibody (HPA020563) used for immunohistochemistry was from Sigma Aldrich (Zwijndrecht, The Netherlands) and the Aven antibody (2300S) used for Western blot was from Cell Signalling (Bioké, Leiden, The Netherlands). The antibody against phospho-ATR(Ser428) (2853) was from Cell Signaling (Bioké, Leiden, Netherlands). The antibody against tubulin (T-9026) was from Sigma-Aldrich (Zwijndrecht, Netherlands). Antibodies against phospho-H3(ser10) (9701), phospho-CHK2(Thr68) (2661P), phospho-H2Ax(Ser139) (9718), phospho-ATM(Ser1981) (5883), and CHK1 (2345) were from Cell Signaling (Bioké, Leiden, Netherlands). The antibody against phospho-CHK1(Ser317) (A300-163A) was from Bethyl Laboratories (Uithoorn, The Netherlands).

Microarray data analysis. Gene expression profiles were obtained from a previously published microarray data set [15]. Kaplan Meier curves were created from the entry “Mixed Osteosarcoma-Kuijer-127-vst-ilmnhwg6v2” in the web application R2 (http://r2.amc.nl).

Immunohistochemistry on tissue microarrays. Tissue microarrays used in this study were previously constructed and published [16]. All specimens in this study were handled according to the ethical guidelines described in ‘Code for Proper Secondary Use of Human Tissue in The Netherlands’ of the Dutch Federation of Medical Scientific Societies. The slide was deparaffinized, rehydrated and blocked of endogenouse peroxidase. Subsequently, antigen retrieval was performed with citrate pH 6.0. Incubation with antibody was overnight at 4°C at a 1:1000 dilution. As a second step we used Immunologic Poly-HRP-GAM/R/R IgG (DVPO110HRP) and Dako liquid DAB+ Substrate Chromogen System (K3468), after which it was counterstained with hematoxiline. Testis tissue was used as control. Slides were scored independently by two observers (JVMGB and ZB). Staining intensity (0 = absent, 1 = weak, 2

= moderate, 3 = strong) and extent of the staining (0 = 0%, 1 = 1-24%, 2 = 25-49%, 3 = 50-74% and 4 = 75-100%) were assessed. The two values were added to obtain the score sum. Cores where the tissue was lost were excluded from the analysis.

Cell culture. Human osteosarcoma cell lines MOS, U2OS, 143B, ZK58 and KPD used were previously described [17,18]. Cells were grown in RPMI1640 medium supplemented with 10% fetal bovine serum and 25 U/mL penicillin and 25 μg/mL of penicillin-streptomycin. All cells were cultured in a humidified incubator at 37°C with 5% CO_2.

siRNA transfection. Transient knockdown of individual genes was achieved using siGenome SMARTpool siRNAs from Dharmacon, Thermofisher Scientific (Landsmeer, Netherlands). The end concentration of siRNA was 20nM and it was delivered to the cells by INTERFERin siRNA transfection reagent according to the manufacturer's procedures (Polyplus transfection, Leusden, Netherlands). Medium was refreshed 24 hours post transfection and transfected cells were used in experiments 48 hours post transfection. The sequences of siRNA are *GAUUAGGGAUGCAGUUAAA, GAACAGGGAAAUUAUUCUA, UAACUGGGAUCGAUAUCAA* and *GUUAUUGGUUCGAGCCCUU*.

Cell cycle analysis. Cell cycle analysis was performed using the Click-iT® Edu Flow Cytometry Assay Kit from Invitrogen (Oregon, USA). Cells were exposed to 10μM 5-ethynyl-2-deoxyuridine (Edu) for 1 hour followed by fixation, permeabilization, and staining. RNAase was added to each sample to a final concentration of 20mg/mL. Edu was probed with Pacific Blue azide and DNA was stained with FxCycle™ Far Red Stain with a final concentration of 200nM.

Immunoblotting. Cells were lysed with SDS protein buffer (125mM Tris/HCl pH 6.8, 20% glycerol, 4% SDS and 0.2% bromophenol blue). Proteins were resolved by SDS-PAGE and transferred to polyvinylidine difluoride membrane. Membranes were blocked in 5% BSA-TBST (TRIS-0.05% Tween20), followed by overnight incubation with primary antibodies and 45 minutes incubation with HRP-conjugated secondary antibodies. Chemoluminescence was detected with a Typhoon 9400 imager (GE Healthcare).

Cell number, cell viability, and real time growth assays. Control or siRNA-transfected cells were treated with compounds for the indicated time points in black 96-well μ-clear plates (Greiner). To determine cell numbers, cells were fixed in 4% paraformaldehyde for 15 minutes and nuclei were stained with Hoechst 33342 for 15 minutes. Plates were imaged

using a BD Pathway 855 imager (Becton Dickinson). Images were processed using an Image-Pro Analyzer 7.0 algorithm, yielding the number of nuclei in each well. For cell viability, cells were processed using the ATPlite 1Step kit (Perkin Elmer) according to the manufacturer's instructions, followed by luminescence measurement on a plate reader. For real time cell growth analysis the RTCA xCELLigence system (Roche Applied Sciences, Almere, The Netherlands) was used. In this system cells are plated on a surface covered with electrodes that measures cell impedance displayed as cell index. Cell index is a quantitative measure of the number of cells present in the well. For the assay, the cells were seeded in an E-View 96 well plate and loaded into the RTCA station immediately. The cells were exposed to compounds 16 hours later, and further monitored for 72 hours. Measurements were taken every 15 minutes.

Real time qPCR. RNA was isolated from control or siRNA-transfected cells using RNeasy (Qiagen). cDNA was generated from 500 ng total RNA using RNeasy Plus Kit from Qiagen. Real time qPCR was performed in triplicate using the SYBRGreen PCRMasterMix (Applied Biosystems) on a 7900HT fast real-time PCRsystem (Applied Biosystems). Primer sequence for CHK1 employed were: forward *TGGTATTGGAATAACTCACAGGGA* and reverse *TGTTCAACAAACGCTCACGA.* Data were collected and analyzed using SDS2.3 software (Applied Biosystems). Relative mRNA levels after correction for GAPDH control mRNA were expressed using 2^(-ΔΔCt) method.

3D culture assay. U2OS and MOS cells were cultured in 384-well plates (Greiner μclear) in a hydrogel containing Matrigel (Beckton Dickinson) and collagen I, supporting invasive growth of both cell lines. Cells in culture were trypsinized and directly added to the cooled gel solution. Using a robotic liquid handler (CyBio Selma 96/60), 14.5μL of gel-cell suspension was transferred to each well of a 384-well plate (2000 cells/well). After polymerization for 30 minutes at 37°C in an atmosphere of 5% CO_2, growth medium was added on top of the gel. After three days, when the cells had formed a network structure, compounds were diluted and added in quadruplicate wells for a period of 72 hours. For measuring cell viability in 3D, a solution of 7g/L WST-1 (Serva Electrophoresis) and 8mg/L phenazinium methylsulfate (PMS; Sigma Aldrich) in 1x PBS were mixed in a 1:1 ratio and 5μL was added to each well. Plates were placed at 37°C for 5 hours, after which the absorbance at 450nm was measured using a FluoStar plate reader. Percentage viability was thereafter calculated by robust normalization (median) of the plates between positive control (no cells; 0% viability) and negative control (solvent; 100% viability) conditions. Results are presented as means ± SD.

For imaging, cells were fixed using 3.7% Formaldehyde (Sigma-Aldrich), permeabilized with 0.1% Triton-X100 and stained for F-actin using 50nM Rhodamine-Phalloidin (Sigma Aldrich) for 12 hours at 4˚C . Subsequently, the plates were washed in PBS for at least 24 hours at 4˚C. The plates were then imaged on a BD Pathway 855 inverted fluorescence microscope (BD Biosciences) using a 4x lens to capture Rhodamine-Phalloidin staining at focal planes spaced 50µm throughout the gel, capturing approximately 70% of a well. Subsequently, maximum intensity projections of the in-focus information of the Z-stacks was made using OcellO (OcellO B.V., Leiden, The Netherlands) image analysis tools.

Synergy assessment. To assess synergy, we used the Bliss independence model, which defines that the effect of a drug at certain concentration is independent of the presence of the other drug.[19] This model predicts the combined response *C* for two single compounds with effects *A* and *B*: $C = A + B - A \bullet B$ [20].

Statistical analysis. Dose response curve fitting and all statistical analyses were performed with GraphPad Prism 5.0 (GraphPad Software, La Jolla, CA). The unpaired two-tailed *t*-test was used to compare between groups. Significant difference between groups in the 3D assay was calculated using 2way ANOVA with Bonferroni posttest.

RESULTS

Aven expression in human osteosarcoma samples

We used a previously published microarray data set[21] with available follow-up data to search for mRNAs whose expression correlated with metastasis-free survival in osteosarcoma patients. We used 53 osteosarcoma samples for which associated survival data were available. These were arranged by Aven mRNA expression level, and the median was used to divide the set in cases with high and low expression. The cutoff set by R2 was 218.6 with a raw p-value of 0.03. Using this approach, high expression of Aven significantly correlated with a lower metastasis-free survival probability (Fig 1A). Next, we assessed Aven protein expression by immunohistochemistry in 31 human primary osteosarcomas and 8 osteosarcoma lung metastases by immunohistochemistry. Aven protein was detected in most samples and expression was significantly higher in metastases as compared to primary osteosarcoma biopsies (Fig 1B,C).

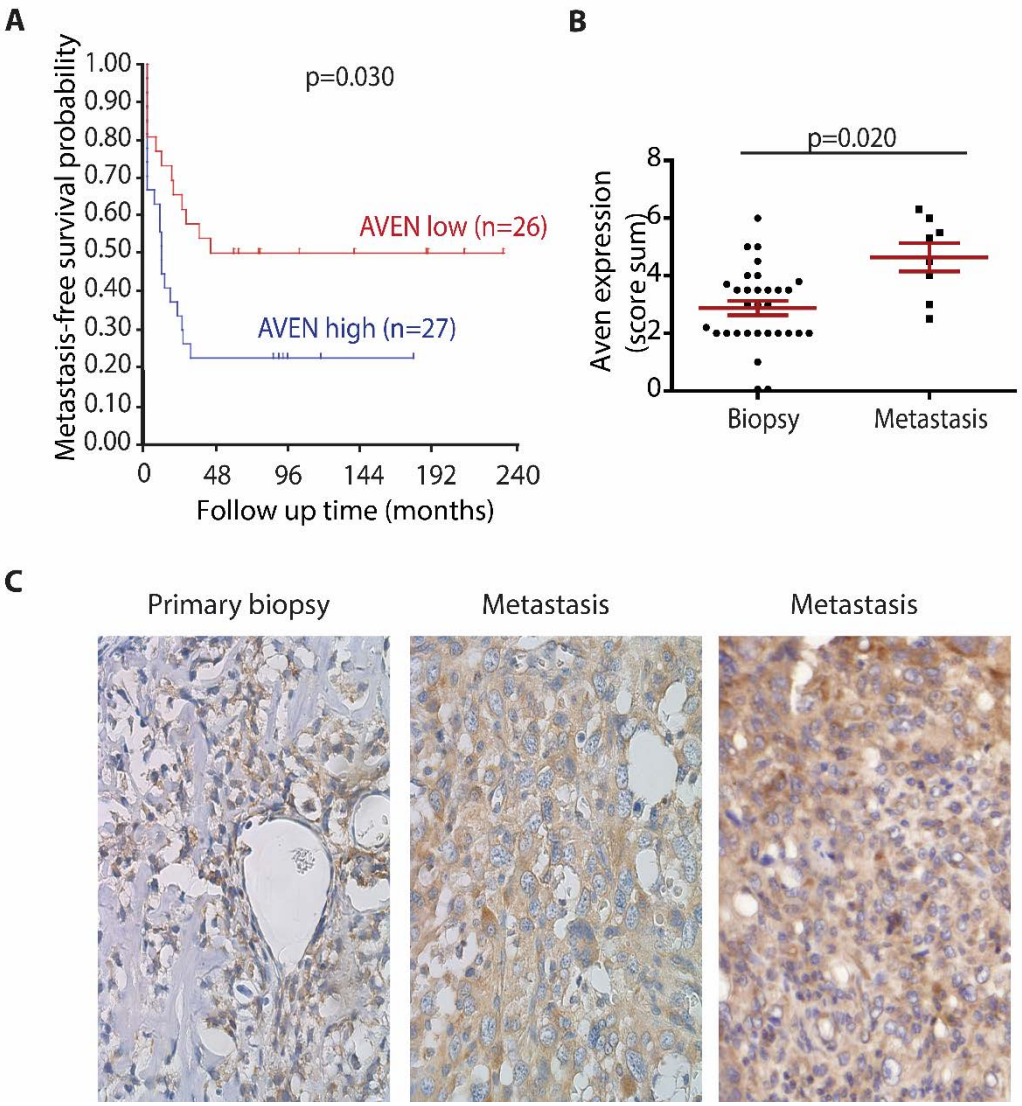

Figure 1. Aven expression in osteosarcoma biopsies. A) Kaplan Meier curve showing relation between Aven mRNA expression and metastasis-free survival. Expression of Aven mRNA was analyzed in 53 samples with survival data, and arranged by expression. The cohort was divided into high and low expression at the median. The curve was made using http://r2.amc.nl. p values were determined by Bonferroni testing. **B)** Sum score of Aven expression in all tumors included in the tissue microarrays. Average is shown in red; p values were determined by two-tailed t test. **C)** Representative images of Aven expression in primary biopsy and metastasis. Images made with 40x Lens.

Aven silencing attenuates growth of human osteosarcoma cells

To determine Aven's role in osteosarcoma cell viability and growth we silenced the *AVEN* gene in two human osteosarcoma cell lines: MOS and U2OS. We used a Smartpool of 4 siRNAs that led to a near complete loss of Aven protein at 48 hours after transfection in both cell lines (Fig 2A). In U2OS cells, transfection with this Smartpool or with any of the four individual siRNAs led to a 60-80% reduction in cell numbers as compared to control, GAPDH-silenced cells (Fig 2B). Likewise, MOS cells transfected with siAven showed a 60% reduction in cell numbers compared to controls (Fig 2C). Aven has been reported to suppress apoptosis in other cell types [4,5,22]. To test if increased apoptosis was responsible for the reduced cell numbers, MOS cells transfected with siAven were treated with the pan-caspase inhibitor, z-VAD-fmk. This led to a slight increase in cell numbers but did not restore growth to that of cells transfected with control siRNAs (Fig 2C). The same results were obtained with U2OS: treatment with z-VAD-fmk did not restore growth of Aven-silenced cells (Fig 2D).

Aven silencing in human osteosarcoma cells triggers G2 cell cycle arrest

We next made use of the RTCA XCelligence system for real time analysis of the effect of Aven silencing on human osteosarcoma cell populations. MOS cells that were MOCK (no siRNA) or siGAPDH transfected, expanded over approximately 24 hours followed by a plateau phase after reaching confluence, whereas siAven-transfected MOS cells stopped expanding at ~18 hours post transfection (Fig 3A). Similarly, a prolonged gradual increase in cell index that was observed for U2OS cells was terminated after 18 hours in response to Aven silencing. This indicated that Aven might be required for effective proliferation of osteosarcoma cells. Indeed, phosphorylation of Histone H3 Ser10 that is associated with mitosis was attenuated in siAven-transfected MOS and U2OS cells, indicating that Aven supported cell cycle progression (Fig 3B). Furthermore, FACS analysis of MOS and U2OS cells pulsed with Edu for 1 hour showed a reduction of cells in S-phase (*t*-test, $p<0.05$) and a concomitant increase in G2 (*t*-test, $p<0.05$) in response to Aven silencing (Fig 3C,D).

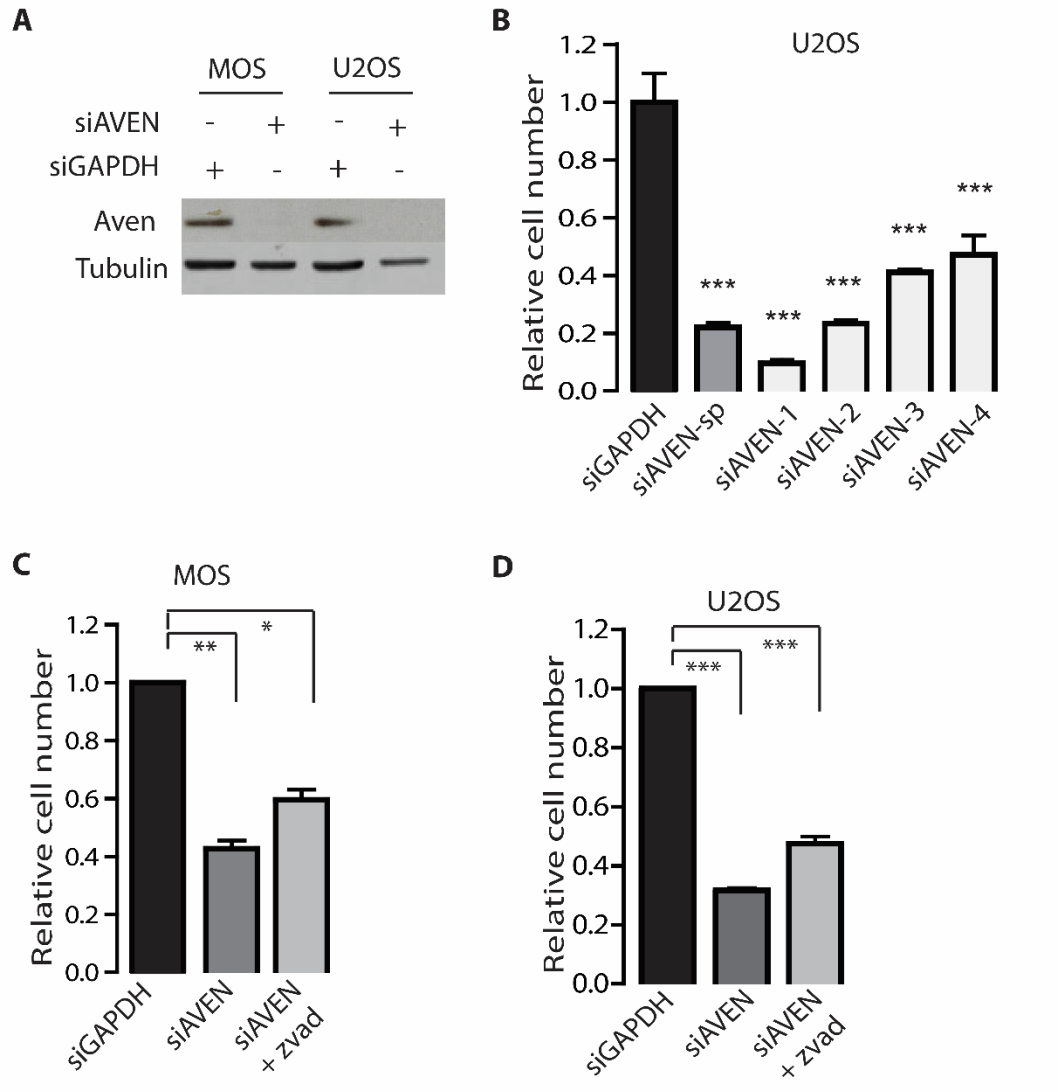

Figure 2. Effect of Aven silencing. A) Western blot analysis of Aven protein abundance and tubulin loading control in MOS and U2OS cells transfected for 48 hours with indicated siRNA Smartpools. **B)** Relative cell numbers based on Hoechst staining, 72 hours post transfection in U2OS cells transfected with GAPDH or Aven siRNA Smartpools or with Aven single siRNAs. Mean +/- SD for experiment performed in quadruplicate is shown. **C**,**D)** Relative cell numbers based on Hoechst staining for MOS and U2OS cell lines, 72 hours post-transfection with indicated siRNA Smartpools. Cells were treated with or without z-VAD-fmk during the last 24 hours (starting at 48 hours post transfection. Mean +/- SEM is shown for three independent experiments done in triplicate. *, $p<0.05$; **, $p<0.01$; ***, $p<0.005$.

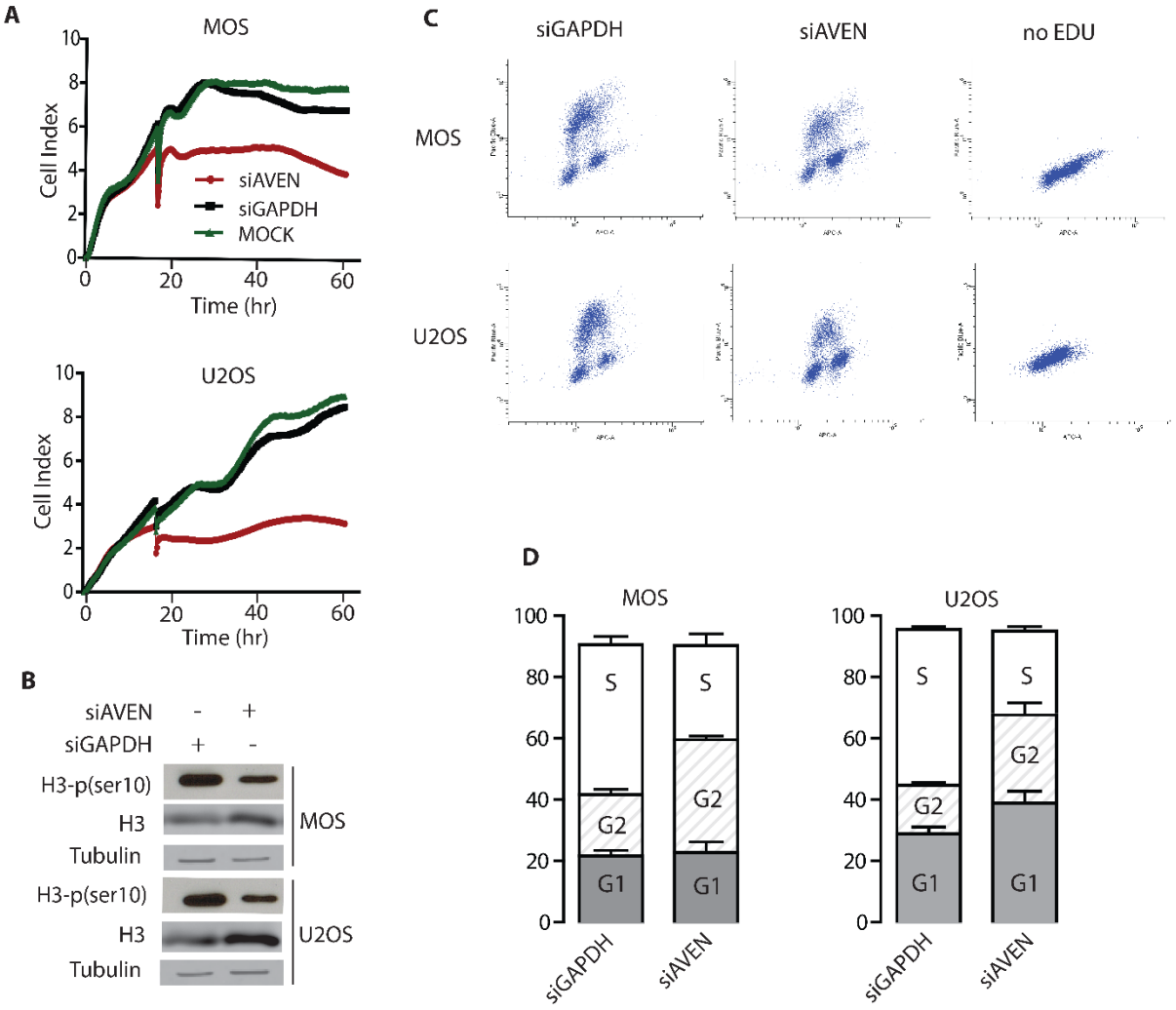

Figure 3. Aven silencing leads to cell cycle arrest. A) Subconfluent cultures of MOS and U2OS cells untransfected (MOCK, green) or transfected with control siGAPDH (black) or siAVEN (red) were monitored for 60 hours with RTCA Xcelligence System. Medium was refreshed at 18 hours post-transfection. Representative experiment of two biological replicates, performed in quadruplicate is shown. **B)** Western blot analysis of total and phospho(Ser10) histone H3 and tubulin loading control for MOS and U2OS cells transfected with siAVEN or siGAPDH for 48 hours. **C)** Flow cytometry analysis of DNA content (x-axis) and Edu incorporation (Y-axis) in MOS and U2OS cells transfected with siAVEN or control siGAPDH pulsed for 1 hour with 10µM Edu after 48 hours. Representative experiment from three biological replicates is shown. **D)** Quantification of data from C. Mean and SEM of three independent experiments is shown.

Aven silencing attenuates ATR-Chk1 DDR signaling in human osteosarcoma cells

The role of Aven in DDR signaling has been attributed to its interaction with ATM [7]. ATM senses double-strand breaks, becomes activated, and subsequently phosphorylates downstream substrates, including Chk2 and p53 [23]. We analyzed ATM activation in U2OS and MOS cells treated for 4 hours with 1 µM doxorubicin. Surprisingly, silencing Aven led to enhanced doxorubicin-induced ATM activation as measured by ATM auto-phosphorylation

at Ser1981 in MOS and U2OS cells (Fig 4A). Chk2 levels increased in response to Aven depletion in these cells (Fig 4B,C). Chk2 phosphorylation at the Thr68 ATM target site was not evident in U2OS cells and in MOS cells doxorubicin triggered ATM Thr68 phosphorylation irrespective of the absence or presence of Aven siRNAs (Fig 4B,C). Likewise, in MOS as well as U2OS cells doxorubicin treatment caused a strong phosphorylation of p53 at the ATM/ATR target site, Ser15 and this response was not affected by Aven silencing (Fig 4B,C).

ATR is activated in response to persistent single-stranded DNA, which is exposed at stalled replication forks and as an intermediate in several DNA damage repair pathways [23]. Doxorubicin treatment caused increased ATR phosphorylation at Ser428 in MOS and U2OS cells, a response that was abolished by Aven silencing (Fig 4A). Moreover, phosphorylation of Chk1 at the ATR target site Ser317 after exposure to doxorubicin was also prevented in Aven-depleted MOS and U2OS cells (Fig 4B,C). This was accompanied by a loss of Chk1 protein accumulation in response to doxorubicin. The role of Aven in the accumulation and phosphorylation of Chk1 was not restricted to doxorubicin but Aven was similarly required for this response in the context of treatment with 5µM cisplatin or 5µM etoposide (Fig 4D). qPCR analysis showed that changes in Chk1 protein abundance were not due to changes in mRNA (Fig S1). Notably, this also excluded a reduction of Chk1 levels through off-target Aven siRNA effects.

Together, these findings indicated that Aven supports ATR-Chk1, but not ATM-Chk2 DDR signaling in osteosarcoma cells. In contrast to ATM-Chk2 signaling, which is particularly important for the response to double strand breaks, ATR-Chk1 signaling is also required for mitotic progression in unperturbed cells [24]. We examined whether the slightly reduced levels of Chk1 (Fig 4B-D) could underlie the cell cycle arrest in Aven-depleted cells. In support of this, silencing Chk1, but not Chk2, impaired MOS cell growth to a similar extent as observed with Aven siRNAs (Fig 2C; S2).

Pharmacological inhibition of Chk1 sensitizes osteosarcoma cells to doxorubicin

Our findings thus far, suggested that Aven-controlled Chk1 signaling might represent an attractive target to sensitize osteosarcoma cells to chemotherapy. Aven inhibitors are not available, but novel Chk1/2 inhibitors that have already been tested in clinical trials are. Therefore, MOS and U2OS cells were treated with a concentration range of the Chk1/2 inhibitor, AZD7762, in combination with a concentration range of doxorubicin. Ranges were based on dose response curves determined for each drug individually (Fig S3,4). Treatment

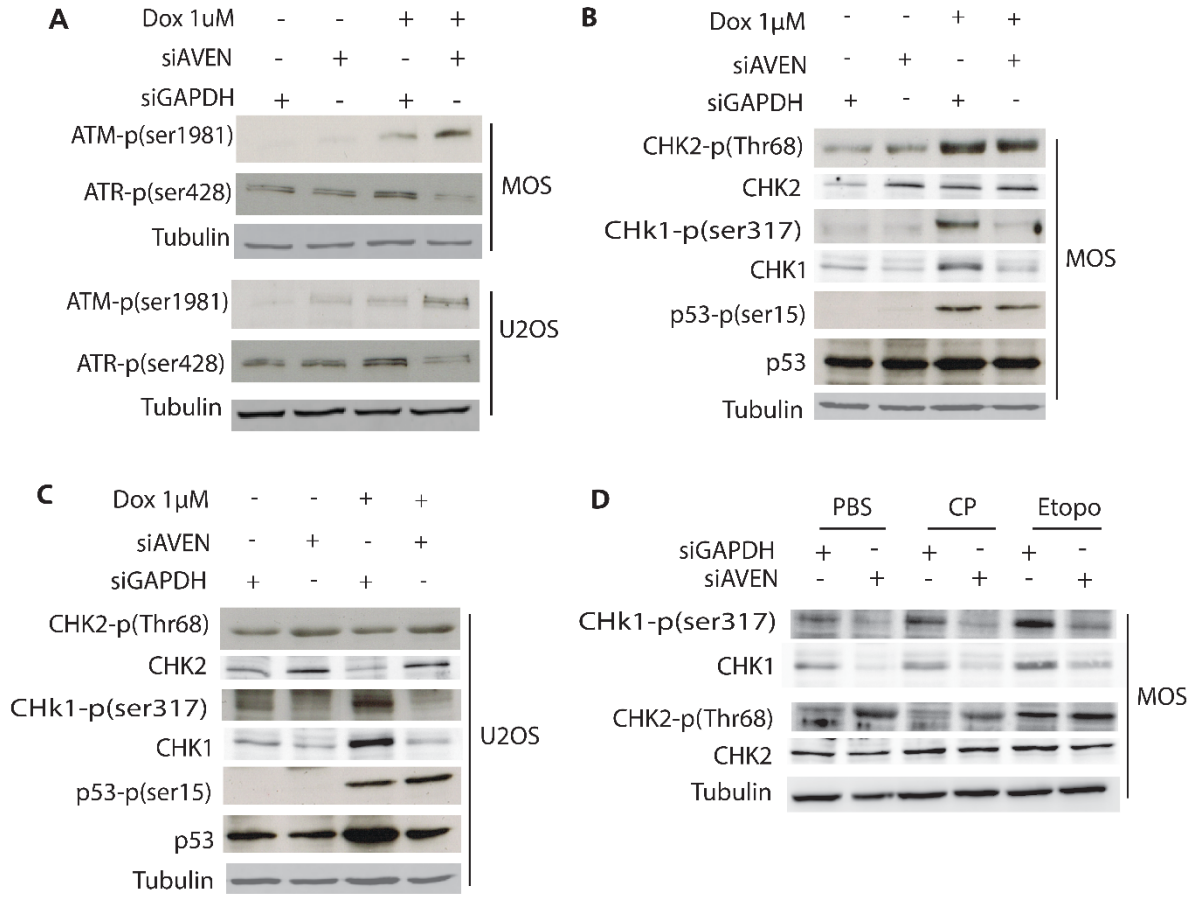

Figure 4. Aven silencing causes shift from ATR-Chk1 to ATM-Chk2 DDR signaling. A) Western blot analysis of total and phospho(Ser1981) ATM, total and phospho(Ser428) ATR, and tubulin loading control for MOS (top) and U2OS cells (bottom) transfected 48 hours with siGAPDH or siAVEN and subsequently treated with 1µM doxorubicin for 4 hours. One representative experiment of 3 is shown. **B**,**C)** Western blot analysis of total and phospho(Thr68) Chk2, total and phospho(Ser317) CHK1, total and phospho(ser15) p53, and tubulin loading control for MOS (**B**) and U2OS cells (**C**) transfected 48 hours with siGAPDH or siAVEN and subsequently treated with 1µM doxorubicin for 4 hours. One representative experiment of 3 is shown. **D)** Western blot analysis of total and phospho(Thr68) Chk2, total and phospho(Ser317) CHK1, and tubulin loading control for MOS cells transfected 48 hours with siGAPDH or siAVEN and subsequently treated with PBS, 5µM cisplatin (CP), or 5µM etoposide for 4 hours.

of MOS with 25-100 nM AZD7762 by itself did not affect cell viability but it led to a strong sensitization to low (50-100 nM) concentrations of doxorubicin (Fig 5A). Calculation of the deviation from additivity as predicted by Bliss independence [19], indicated synergy between AZD7762 and doxorubicin (Fig 5B). The same synergistic relationship between these two compounds was observed for U2OS cells (Fig 5C,D). We further explored the AZD7762-doxorubicin combination using three other human osteosarcoma cell lines, ZK58, KPD, and

143B. Again, 50 nM AZD7762 slightly increased the effect of doxorubicin on ZK58 and strongly sensitized KPD and 143B cells to doxorubicin treatment (Fig 5E).

We also examined the interaction of two clinically relevant selective CHK1 inhibitors, CHIR-124 and LY2603618 with doxorubicin in osteosarcoma cells. CHIR-124 by itself already affected viability at concentrations above 25 nM, especially in U2OS cells (Fig 5F,G). At 25 nM, CHIR-124 sensitized MOS and to a lesser extent, U2OS to doxorubicin (Fig 5F,G; S5). Up to 0.25 µM LY2603618 by itself did not affect either cell line but at this concentration LY2603618 strongly augmented the effect of low concentrations of doxorubicin in U2OS and, especially in MOS cells (Fig 5H,I; S5).

2D and 3D osteosarcoma cultures are chemosensitized by Chk1 inhibition

We confirmed chemosensitization by Chk inhibition by monitoring the cells over a period of 96 hours using the xCELLigence system. Growth of U2OS cells exposed to 0.1 µM doxorubicin was similar to growth under control conditions whereas treatment with 0.5 µM doxorubicin caused a loss of cells (Fig 6A). Again, exposure to 50 nM AZD7762 had no effect by itself but effectively sensitized U2OS cells to 0.1 µM doxorubicin (Fig 6A).

We further validated the possibility of chemosensitization by Chk1 inhibition using 3D osteosarcoma cell cultures. MOS and U2OS cells were suspended in a mixture of collagen and matrigel and allowed to grow for three days. Subsequently, cultures were exposed to a dose rage of doxorubicin in the absence or presence of 50 nM AZD7762, 25nM CHIR-124, or 0,125µM LY2603618 for 72 hours and viability was determined using a biochemical assay. Similar to the results in 2D cultures, MOS and to a lesser extent U2OS were sensitized in 3D to low doses of doxorubicin when Chk1/2 was inhibited using AZD7762 (Fig 6B,C).

Likewise, 3D cultures of U2OS and especially MOS were effectively sensitized to doxorubicin by the two selective Chk1 inhibitors CHIR-124 and LY2603618 (Fig 6B,C). Moreover, image-based analysis at the same time as biochemical viability assessment showed that combined exposure to 50nM AZD7762 and 0.05µM doxorubicin caused disruption of the multicellular network, which was not seen when either of these drugs was used alone (Fig 6D).

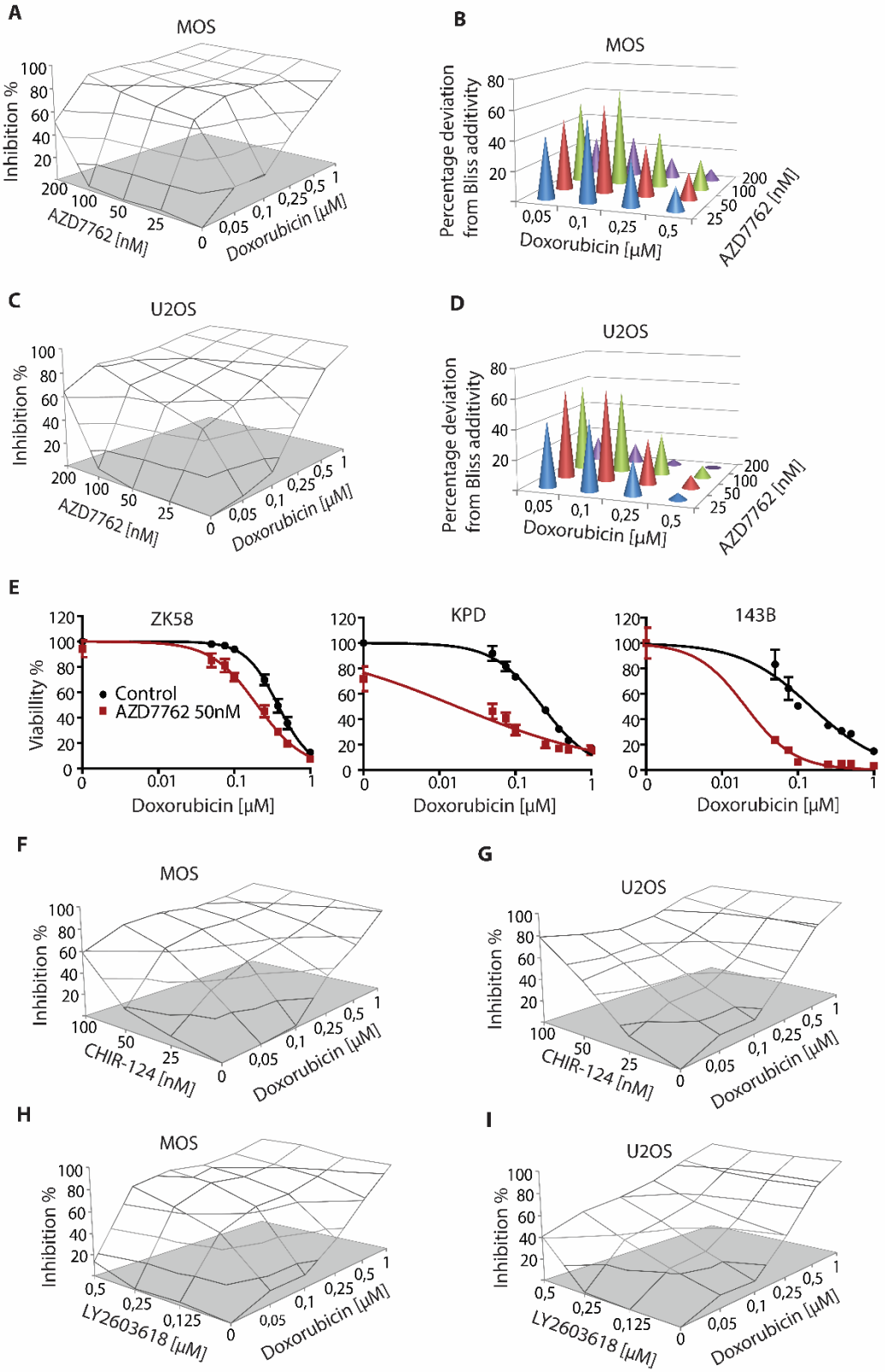

Figure 5. Treatment with Chk1 inhibitor sensitizes osteosarcoma cells to doxorubicin.

A,C) Combined effect of doxorubicin and AZD7762 dose ranges in MOS (**A**) and U2OS cell (**C**). Mean of triplicates is shown. Each graph shows one representative of three independent experiments. **B,D)** Needle graphs showing deviation from Bliss-predicted additivity based on data shown in A,C. Mean of triplicates is shown. Each graph shows one representative of three independent experiments. **E)** Doxorubicin dose response curves for three human osteosarcoma cell lines as indicated in absence or presence of 50nM of AZD7762. Cells were exposed for 72 hours. Each graph represents mean ± SEM. **F,G)** Combined effect of doxorubicin and CHIR-124 dose ranges in MOS (**F**) and U2OS (**G**) cells. Mean of triplicates is shown. Each graph shows one representative of three independent experiments. **H,I)** Combined effect of doxorubicin and LY2603618 dose ranges in MOS (**H**) and U2OS (**I**) cells. Mean of triplicates is shown. Each graph shows one representative of three independent experiments.

DISCUSSION

Our data point to a role for Aven in growth and therapy resistance of osteosarcomas. High expression of Aven mRNA correlates with low metastasis-free survival in conventional osteosarcoma patients and Aven protein expression is high in metastasis as compared to primary biopsies of osteosarcoma. Aven has been shown to suppress apoptosis through its ability to enhance the anti-apoptotic effect of BCL-xl and to interfere with Apaf-1-mediated apoptosome formation in leukemic and breast cancer cells [4,5,14]. In human osteosarcoma cells we find that depletion of Aven does not trigger cell death through apoptosis. Rather, it leads to a G2 cell cycle arrest and ultimately to loss of viability by a mechanism that is not caspase-dependent. Instead, our findings indicate that this is due to impaired checkpoint kinase signaling.

Checkpoint kinases Chk1 and Chk2 coordinate progression through the cell cycle[23,25] and Chk1 is expressed in S through M phase of the cell cycle [26]. Aven-depleted osteosarcoma cells have reduced phospho-Chk1(Ser317) and total Chk1 protein levels. Thus, Aven supports Chk1 protein synthesis or stability. As Ser317-phosphorylated Chk1 is required for DNA replication and mitotic progression [24], the important role we identify for Aven in osteosarcoma cell proliferation can be explained by its support of Chk1 abundance and phosphorylation.

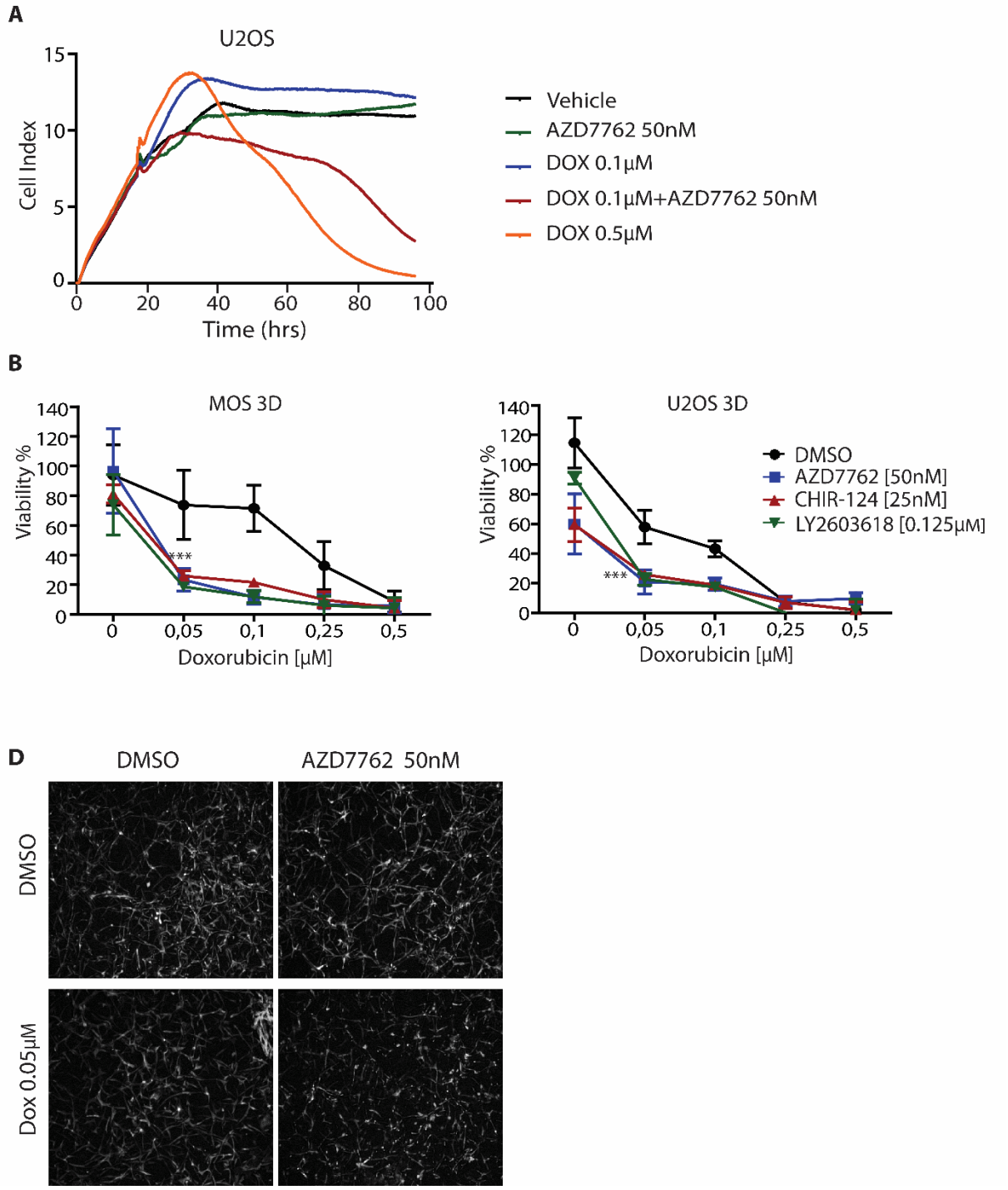

Figure 6. Osteosarcoma cells are sensitized to doxorubicin by Chk1 inhibition in a 2D and 3D environment. A) Subconfluent U2OS cultures were monitored for 90 hours with RTCA Xcelligence System. Cells were exposed 16 hours after seeding to vehicle (black line), 50nM AZD7762 (green line), 0.1µM doxorubicin (blue line), 0.5 µM doxorubicin (orange line), or 0.1µM doxorubicin in combination with 50nM AZD7762 (red line). One experiment of two independent experiments done in quadruplicate is shown. **B,C)** Cell viability measured by WST assay in 3D extracellular matrix-embedded MOS (**B**) and U2OS cultures (**C**) grown for 3 days and subsequently exposed to indicated compound concentrations for 72 hours. Mean ± SD of triplicates (MOS cells) or quadruplicates (U2OS cells) are shown. **D)** Representative images of 3D cultures of MOS cells exposed to DMSO, 50nM

AZD7762, 0.05µM doxorubicin, or the combination of the two drugs. Images are compressed z-stacks of actin cytoskeletal staining (Rhodamine-Phalloidin).

The anti-apoptotic role of Aven is especially prominent in the response to genotoxic therapy. Overexpression of Aven in leukemic and breast cancer cells promotes resistance to γ irradiation and DNA damaging agents such as UV, SN-38 and cisplatin [4,5]. In addition to its role in BCL-xl function and interference with Apaf-1-mediated apoptosome formation as discussed above, this may be related to its role in DDR signaling. Aven has been shown to support ATM activation in cycling *Xenopus* eggs and in HeLa cells treated with neocarzinostatin [7]. Remarkably, our findings demonstrate that ATM activation in response to doxorubicin is fully intact or even potentiated in Aven-silenced osteosarcoma cells. Instead, we show that ATR activation in response to genotoxic stress is abrogated in the absence of Aven.

ATM is mainly activated by double strand breaks, subsequently activating Chk2 to induce cell cycle arrest or apoptosis when the damage is extensive [9]. ATR is an essential regulator of genome integrity, responding to various types of DNA damage and it activates Chk1 [8]. However, crosstalk between ATM and ATR occurs and Chk1 activation by ATR in the context of double strand breaks is dependent on ATM [27,28]. Our data implicate Aven in ATR-Chk1 activation under conditions of genotoxic stress whereas baseline ATR Ser428 phosphorylation appears unaffected by Aven silencing. This suggests that Aven may facilitate the interaction between ATM and ATR, driving ATR signaling in response to double strand breaks.

We show that in osteosarcoma cells, the absence of Aven shifts the DDR from ATR-Chk1 to ATM-Chk2 signaling. This does not affect the activation of p53 in response to genotoxic stress. In U2OS cells expressing wild type p53 as well as in MOS cells expressing a mutant p53, silencing Aven does not affect phosphorylation of p53 at the ATM/ATR target site Ser15 in response to doxorubicin. Under these conditions, ATM, either directly or through Chk2 likely phosphorylates p53 at Ser15 in response to DNA damage [29].

As a potential scaffold protein without enzymatic activity, Aven is unlikely to represent a candidate drug target. However, our data show that Aven-controlled Chk1 signaling may well be an interesting drug target in osteosarcoma. Depletion of Chk1, but not Chk2, to some extent phenocopies the effect of Aven silencing and pharmacological inhibition of Chk1 at higher compound concentrations has the same effect. The use of Chk1

inhibitors for osteosarcoma appears most promising in a combination strategy. Chk1 inhibition is already used as a therapeutic approach to potentiate the efficacy of genotoxic chemotherapeutics in other cancer types [30].

The Chk1/Chk2 inhibitor, AZD7762, is known to potentiate the effect of cisplatin in ovarian clear cell carcinoma [31] as well as in multiple myeloma cells [32]. It was also reported to sensitize pancreatic tumor cells to radiation and to interfere with DNA repair in these cells [33]. However, recently it was reported that this drug would not be continued in clinical trials due to cardiac toxicity [34]. We have tested two selective Chk1 inhibitors, CHIR-124 and LY2603618. The latter drug was tested in a phase I dose-escalation study, and acceptable safety and pharmacokinetic profiles were reported [35,36]. Here, in 2D as well as 3D cultures of human osteosarcoma cells, low concentrations of Chk1 inhibitors cause effective sensitization to low concentrations of doxorubicin. Doxorubicin is routinely used in the treatment of osteosarcoma patients but resistance is a major obstacle [37]. Our findings indicate that abrogation of Chk1 signaling using clinically relevant drugs may be combined with chemotherapy to more effectively treat osteosarcoma.

ACKNOWLEDGEMENTS

The authors would like to thank Jan Koster for help with R2, Inge Briaire-de Bruijn for immunohistochemistry and technical advice, Yvonne de Jong for designing the qPCR primers for CHK1, and Laura Heitman for her introduction to the xCELLigence System. This project was granted by a university profile grant of Leiden University/LUMC titled “Translational Drug Discovery and Development”.

AUTHOR CONTRIBUTION

ZB conceived and carried out experiments, THB carried out and analyzed the 3D assay. All authors were involved in writing the paper and had final approval of the submitted and published versions.

REFERENCES

1. Anninga JK, Gelderblom H, Fiocco M*, et al.* Chemotherapeutic adjuvant treatment for osteosarcoma: where do we stand? *Eur J Cancer* 2011; **47**: 2431-2445.
2. Fletcher CDM, Bridge JA, Hogendoorn PCW*, et al.* Conventional osteosarcoma. In: WHO Classification of Tumours of Soft Tissue and Bone. (ed)^(eds). IARC: Lyon, 2013; 282-288.
3. Buddingh EP, Anninga JK, Versteegh MI*, et al.* Prognostic factors in pulmonary metastasized high-grade osteosarcoma. *Pediatric blood & cancer* 2010; **54**: 216-221.
4. Chau BN, Cheng EH, Kerr DA*, et al.* Aven, a novel inhibitor of caspase activation, binds Bcl-xL and Apaf-1. *Mol Cell* 2000; **6**: 31-40.
5. Kutuk O, Temel SG, Tolunay S*, et al.* Aven blocks DNA damage-induced apoptosis by stabilising Bcl-xL. *Eur J Cancer* 2010; **46**: 2494-2505.
6. Hawley RG, Chen Y, Riz I*, et al.* An Integrated Bioinformatics and Computational Biology Approach Identifies New BH3-Only Protein Candidates. *Open Biol J* 2012; **5**: 6-16.
7. Guo JY, Yamada A, Kajino T*, et al.* Aven-dependent activation of ATM following DNA damage. *Curr Biol* 2008; **18**: 933-942.
8. Mordes DA, Cortez D. Activation of ATR and related PIKKs. *Cell Cycle* 2008; **7**: 2809-2812.
9. Kurz EU, Lees-Miller SP. DNA damage-induced activation of ATM and ATM-dependent signaling pathways. *DNA Repair (Amst)* 2004; **3**: 889-900.
10. Bartek J, Lukas J. Chk1 and Chk2 kinases in checkpoint control and cancer. *Cancer Cell* 2003; **3**: 421-429.
11. Garrett MD, Collins I. Anticancer therapy with checkpoint inhibitors: what, where and when? *Trends Pharmacol Sci* 2011; **32**: 308-316.
12. Paydas S, Tanriverdi K, Yavuz S*, et al.* Survivin and aven: two distinct antiapoptotic signals in acute leukemias. *Ann Oncol* 2003; **14**: 1045-1050.
13. Choi J, Hwang YK, Sung KW*, et al.* Aven overexpression: association with poor prognosis in childhood acute lymphoblastic leukemia. *Leuk Res* 2006; **30**: 1019-1025.
14. Eissmann M, Melzer IM, Fernandez SB*, et al.* Overexpression of the anti-apoptotic protein AVEN contributes to increased malignancy in hematopoietic neoplasms. *Oncogene* 2013; **32**: 2586-2591.
15. Kuijjer ML, Rydbeck H, Kresse SH*, et al.* Identification of osteosarcoma driver genes by integrative analysis of copy number and gene expression data. *Genes Chromosomes Cancer* 2012; **51**: 696-706.
16. Mohseny AB, Szuhai K, Romeo S*, et al.* Osteosarcoma originates from mesenchymal stem cells in consequence of aneuploidization and genomic loss of Cdkn2. *J Pathol* 2009; **219**: 294-305.
17. Mohseny AB, Machado I, Cai Y*, et al.* Functional characterization of osteosarcoma cell lines provides representative models to study the human disease. *Lab Invest* 2011; **91**: 1195-1205.
18. Ottaviano L, Schaefer KL, Gajewski M*, et al.* Molecular characterization of commonly used cell lines for bone tumor research: a trans-European EuroBoNet effort. *Genes Chromosomes Cancer* 2010; **49**: 40-51.

19. Greco WR, Bravo G, Parsons JC. The search for synergy: a critical review from a response surface perspective. *Pharmacol Rev* 1995; **47**: 331-385.
20. Borisy AA, Elliott PJ, Hurst NW*, et al.* Systematic discovery of multicomponent therapeutics. *Proc Natl Acad Sci U S A* 2003; **100**: 7977-7982.
21. Kuijjer ML, Hogendoorn PC, Cleton-Jansen AM. Genome-wide analyses on high-grade osteosarcoma: making sense of a genomically most unstable tumor. *Int J Cancer* 2013; **133**: 2512-2521.
22. Figueroa B, Jr., Chen S, Oyler GA*, et al.* Aven and Bcl-xL enhance protection against apoptosis for mammalian cells exposed to various culture conditions. *Biotechnol Bioeng* 2004; **85**: 589-600.
23. Kastan MB, Bartek J. Cell-cycle checkpoints and cancer. *Nature* 2004; **432**: 316-323.
24. Wilsker D, Petermann E, Helleday T*, et al.* Essential function of Chk1 can be uncoupled from DNA damage checkpoint and replication control. *Proc Natl Acad Sci U S A* 2008; **105**: 20752-20757.
25. OncogeneBartek J, Falck J, Lukas J. CHK2 kinase--a busy messenger. *Nat Rev Mol Cell Biol* 2001; **2**: 877-886.
26. Kaneko YS, Watanabe N, Morisaki H*, et al.* Cell-cycle-dependent and ATM-independent expression of human Chk1 kinase. *Oncogene* 1999; **18**: 3673-3681.
27. Jazayeri A, Falck J, Lukas C*, et al.* ATM- and cell cycle-dependent regulation of ATR in response to DNA double-strand breaks. *Nat Cell Biol* 2006; **8**: 37-45.
28. Cuadrado M, Martinez-Pastor B, Murga M*, et al.* ATM regulates ATR chromatin loading in response to DNA double-strand breaks. *J Exp Med* 2006; **203**: 297-303.
29. Harper JW, Elledge SJ. The DNA damage response: ten years after. *Mol Cell* 2007; **28**: 739-745.
30. McNeely S, Beckmann R, Bence Lin AK. CHEK again: revisiting the development of CHK1 inhibitors for cancer therapy. *Pharmacol Ther* 2014; **142**: 1-10.
31. Itamochi H, Nishimura M, Oumi N*, et al.* Checkpoint kinase inhibitor AZD7762 overcomes cisplatin resistance in clear cell carcinoma of the ovary. *Int J Gynecol Cancer* 2014; **24**: 61-69.
32. Landau HJ, McNeely SC, Nair JS*, et al.* The checkpoint kinase inhibitor AZD7762 potentiates chemotherapy-induced apoptosis of p53-mutated multiple myeloma cells. *Mol Cancer Ther* 2012; **11**: 1781-1788.
33. Morgan MA, Parsels LA, Zhao L*, et al.* Mechanism of radiosensitization by the Chk1/2 inhibitor AZD7762 involves abrogation of the G2 checkpoint and inhibition of homologous recombinational DNA repair. *Cancer Res* 2010; **70**: 4972-4981.
34. Sausville E, Lorusso P, Carducci M*, et al.* Phase I dose-escalation study of AZD7762, a checkpoint kinase inhibitor, in combination with gemcitabine in US patients with advanced solid tumors. *Cancer Chemother Pharmacol* 2014; **73**: 539-549.
35. Weiss GJ, Donehower RC, Iyengar T*, et al.* Phase I dose-escalation study to examine the safety and tolerability of LY2603618, a checkpoint 1 kinase inhibitor, administered 1 day after pemetrexed 500 mg/m(2) every 21 days in patients with cancer. *Invest New Drugs* 2013; **31**: 136-144.
36. Calvo E, Chen VJ, Marshall M*, et al.* Preclinical analyses and phase I evaluation of LY2603618 administered in combination with Pemetrexed and cisplatin in patients with advanced cancer. *Invest New Drugs* 2014; **5**: 955-968.

37. Luetke A, Meyers PA, Lewis I*, et al.* Osteosarcoma treatment - where do we stand? A state of the art review. *Cancer Treat Rev* 2014; **40**: 523-532.

Supplementary Figures

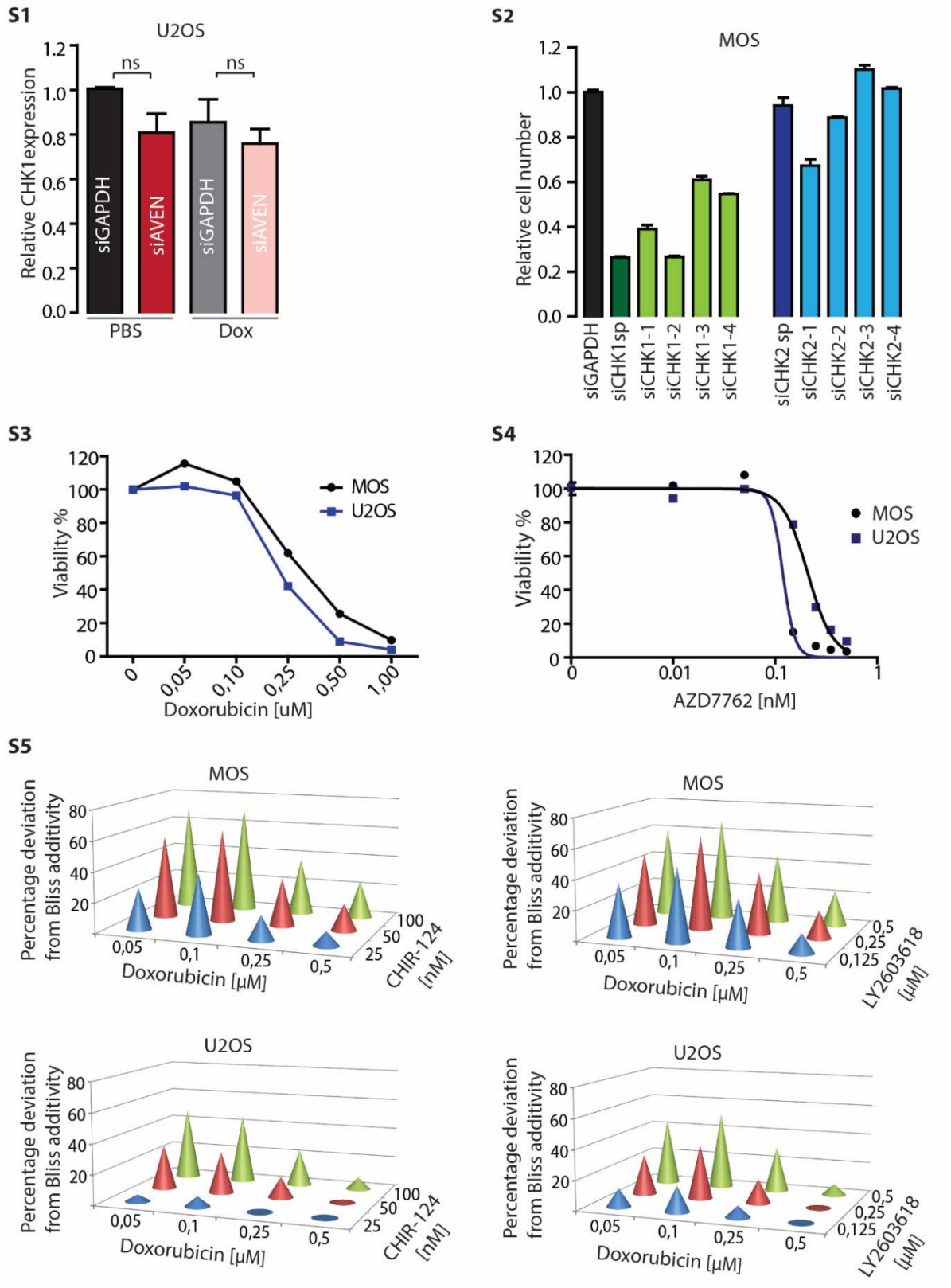

Figure S1) qPCR analysis showing Chk1 mRNA levels in U2OS cells transfected 48 hours with the indicated siRNAs. Mean +/- SEM of 3 independent experiments done in triplicate is shown.

Figure S2) MOS cells were transfected with siGAPDH, siChk1, siChk2 for 72 hours and cell numbers were determined by HOECHST staining and nuclei counting.
Figure S3) Dose response curve of Doxorubicin in MOS and U2OS cells; 72 hours exposure. Mean +/- S.D of one experiment done in triplicate.
Figure S4) Dose response curve of AZD7762 in MOS (black line) and U2OS cells (blue line); 72 hours exposure. Mean +/- SEM of 3 independent experiments done in triplicate is shown.
Figure S5) Needle graphs showing deviation from Bliss-predicted additivity in MOS (top) and U2OS cells (bottom) exposed to doxorubicin and CHIR-124 dose ranges (left) or doxorubicin and LY2603618 dose ranges (right). Each graph shows one representative of three independent experiments performed in triplicate.